Journal of Solid State Chemistry **165,** 334–344 (2002)
doi:10.1006/jssc.2002.9547, available online at http://www.idealibrary.com on IDEAL®

Synthesis of Open-Framework Iron Phosphates, $[C_6N_2H_{14}][Fe^{III}_2F_2(HPO_4)_2(H_2PO_4)_2]\cdot 2H_2O$ and $[C_6N_2H_{14}]_2[Fe^{III}_3(OH)F_3(PO_4)(HPO_4)_2]_2\cdot H_2O$, with One- and Three-Dimensional Structures

S. Mahesh,* Mark A. Green,† and Srinivasan Natarajan*,[1]

** Framework Solids Laboratory, Chemistry and Physics of Materials Unit, Jawaharlal Nehru Centre for Advanced Scientific Research, Jakkur P.O., Bangalore 560 064, India, and † Davy-Faraday Research Laboratory, The Royal Institution of Great Britain, 21 Albemarle Street, London W1S 4BS, United Kingdom*

Received October 29, 2001; in revised form February 5, 2002; accepted February 15, 2002

The hydrothermal syntheses and structures of two new open-framework iron phosphates, I, $[C_6N_2H_{14}][Fe^{III}_2F_2(HPO_4)_2(H_2PO_4)_2].2H_2O$, II, and $[C_6N_2H_{14}]^2[Fe^{III}_3(OH)F_3(PO_4)(HPO_4)_2]_2.H_2O$, are presented. The structures of both I and II consist of FeO^4F^2 octahedra and PO_4 terahedra linked to form one- and three-dimensional structures. Both the compounds possess infinite one-dimensional chains of Fe–O/F–Fe formed by the FeO_4F_2 octahedra. The di-protonated DABCO cations are located in between the chains in I and within the channels in II. Whilst I possess the tancoite structure with a new chain composition, II has a three-dimensional structure similar to the gallophosphate, ULM-1. Crystal data for I: $M = 685.84$, monoclinic, space group = $C2/c$ (no. 15), $a = 7.232(2)$, $b = 20.520(7)$, $c = 13.933(4)$ Å, $\beta = 97.68(3)^\circ$, $v = 2049.1(1)$ Å^3, $Z = 4$, $\rho_{calc.} = 2.223$ g cm^{-3}, $\mu(MoK\alpha) = 1.841$ mm^{-1}, $R_1 = 0.06$, $wR_2 = 0.12$, $S = 1.17$ for 163 parameters; II, $M = 1303.33$, monoclinic, space group = $C2/c$ (no. 15), $a = 18.1836(2)$, $b = 10.0126(7)$, $c = 20.0589(4)$ Å, $\beta = 106.08(3)^\circ$, $v = 3509.0(2)$ Å^3, $Z = 4$, $\rho_{calc} = 2.467$ gcm^{-3}, $\mu(MoK\alpha) = 2.830$ mm^{-1}, $R_1 = 0.034$, $wR_2 = 0.081$, $S = 1.06$ for 284 parameters. © 2002 Elsevier Science (USA)

INTRODUCTION

Solids possessing extended architectures are being studied for their many applications in the areas of catalysis, sorption and separation processes. Thus, during the last decade or so large number of new materials with novel architectures have been synthesized and characterized (1). These solids are, in general, synthesized hydrothermally in the presence of organic amines. The organic amine molecules occupy voids, cavities and channels in these solids and can be removed, in some cases, by post-synthesis treatment such as calcinations, acid-leaching, etc.

Although designing phases similar to aluminosilicate zeolitic structures continues to be the main interest in the area of open-framework materials, the discovery of new solids with novel structural features has also assumed an important role (1). Among the open-framework materials, metal phosphates occupy a prime position. Of these, transition metal phosphates especially those of iron constitute an important family (2–10). Thus, iron phosphates with one- (3), two- (4–6) and three-dimensional (7–10) architectures have been synthesized and characterized.

Open-framework iron phosphates reported in the literature are generally synthesized hydrothermally starting from simple salts of iron, such as chloride or nitrate, in the presence of phosphoric acid and an organic amine. Recently, it was shown that the use of metal complexes in the synthesis mixture provides a facile method for the preparation of new types of open-framework phosphates with novel architectures (11). The metal complexes probably release the metal ions slowly into the solution, during the hydrothermal crystallization, thereby facilitating the formation of such new structures. We have employed similar approaches for the preparation of novel iron phosphates forming new materials with open architectures (7b, 7c). In continuation of this theme, we have been investigating the formation of iron phosphates using iron acetylacetonate, $[Fe(acac)_3]$, as the starting source for iron in the presence of 1,4-diazabicyclo[2,2,2]octane (DABCO) employing hydrothermal methods. In this paper, we report the synthesis and structural characterization of two new iron phosphates, $[C_6N_2H_{14}][Fe^{III}_2F_2(HPO_4)_2(H_2PO_4)_2]\cdot 2H_2O$, **I**, and $[C_6N_2H_{14}]_2[Fe^{III}_3(OH)F_3(PO_4)(HPO_4)_2]_2\cdot H_2O$, **II**, with one- and three-dimensional structure. Whilst **I** has the tancoite structure (12), **II** has the structure of the gallium

[1] To whom correspondence should be addressed. Fax: (+)-91-80-846-2766. E-mail: raj@jncasr.ac.in.

0022-4596/02 $35.00

phosphate, $[C_6N_2H_{14}]_2[Ga_3(OH)F_3(PO_4)(HPO_4)_2]_2 \cdot H_2O$, designated as ULM-1 (13).

EXPERIMENTAL

Compounds **I** and **II** were synthesized under hydrothermal conditions starting from a coordination complex of Fe^{3+}, $[Fe(acac)_3]$ as the source of iron. In a typical synthesis of **I**, 0.45 g of $Fe(acac)_3$ was dispersed in 9.2 mL of deionized water. To this 0.7 mL of H_3PO_4 (85 wt%) and 0.37 mL of HF (48%w/w) was added under continuous stirring. Finally, 0.572 g of DABCO was added to the above and the mixture was homogenized for 20 min at room temperature. The final orange-colored liquid with the composition, $Fe(acac)_3 : 8.6H_3PO_4 : 4DABCO : 8HF : 400H_2O$, was transferred and sealed in a 23 mL PTFE-lined stainless-steel autoclave and heated at 150°C for 120 h. The resulting product, a mixture of black powder and few colorless crystals, were vacuum filtered and washed with plenty of deionized water and dried at ambient conditions. The single crystals could be easily separated from the powder under a polarizing microscope. The black powder was found to be a condensed iron phosphate, $Fe(PO_4)$. In order to prepare **I** in pure phase, a reaction mixture of the composition, $Fe(acac)_3{:}4H_3PO_4{:}2DABCO{:}4HF{:}200H_2O$ was heated at 100°C for 96 h, resulting in single phasic polycrystalline powder of **I**. The same synthesis mixture, when heated at 150°C for 48 h, resulted in large quantities of colorless single crystals of **II**. In both the cases, the initial pH of the reaction mixture was found to be around 2 and no appreciable change in the pH has been noted after the reaction. An EDAX analysis indicated an Fe:P ratio of 1:2 for **I** and 1:1 for **II**, in addition to indicating the presence of fluorine. A chemical analysis also confirmed the presence of fluorine (obs. 5.2%, calc. 5.6% for **I** and obs. 3%, calc. 3.26% for **II**) (14). The compounds **I** and **II** were characterized by powder X-ray diffraction (XRD), and thermogravimetric analysis (TGA).

Thermogravimetric analysis of compounds **I** and **II** were carried out in flowing nitrogen (50 mL/min^{-1}) in the range

TABLE 1
Summary of Crystal Data, Intensity Measurements and Structure Refinements Parameters for I, $[C_6N_2H_{14}][Fe^{III}{}_2F_2(HPO_4)_2(H_2PO_4)_2] \cdot 2H_2O$, II, and $[C_6N_2H_{14}]_2[Fe^{III}{}_3(OH)F_3(PO_4)(HPO_4)_2]_2 \cdot H_2O$

Parameter	I	II
Empirical formula	$Fe_2P_4F_2O_{18}C_6N_2H_{24}$	$Fe_6P_6F_6O_{27}C_{12}N_4H_{36}$
Crystal system	Monoclinic	Monoclinic
Space group	$C2/c$ (no. 15)	$C2/c$ (no. 15)
Crystal size (mm)	$0.24 \times 0.16 \times 0.16$	$0.2 \times 0.12 \times 0.08$
a (Å)	7.232(2)	18.1836(6)
b (Å)	20.520(7)	10.0126(4)
c (Å)	13.933(4)	20.0589(6)
β (°)	97.68(3)	106.08(9)
Volume (Å^3)	2049.1(1)	3509.0(2)
Z	8	8
Formula mass	685.84	1303.33
ρ_{calc} (g cm^{-3})	2.223	2.467
λ (Mo$K\alpha$) Å	0.71073	0.71073
μ (mm^{-1})	1.841	2.830
2θ range (°)	4–46.5	4–46.5
Total data collected	4219	7086
Index ranges	$-8 \le h \le 7$, $-22 \le h \le 18$, $-15 \le l \le 15$	$-20 \le h \le 19$, $-11 \le h \le 10$, $-16 \le l \le 22$
Unique data	1466	2517
Observed data ($I > 2\sigma(I)$)	1106	2038
Refinement method	Full-matrix least squares on $\|F^2\|$	Full-matrix least squares on $\|F^2\|$
R_{merg}	0.0858	0.035
R indexes [I > 2σ(I)]	$R_1 = 0.060$,[a] w$R_2 = 0.120$[b]	$R_1 = 0.034$, w$R_2 = 0.081$
R (all data)	$R_1 = 0.084$, w$R_2 = 0.135$	$R_1 = 0.048$, w$R_2 = 0.089$
Goodness of fit ($S_{obs.}$)	1.174	1.063
No. of variables	163	284
Largest difference map peak and hole (Å^{-3})	1.058 and -0.442	0.512 and -0.505

[a] $R_1 = \sum ||F_o| - |F_c|| / \sum |F_o|$.

[b] w$R_2 = \{\sum[w(F_o^2 - F_c^2)^2] / \sum[w(F_o^2)^2]\}^{1/2}$. $w = 1/[\sigma^2(F_o)^2 + (aP)^2 + bP]$, $P = [\max.(F_o^2,0) + 2(F_c)^2]/3$, where $a = 0.0274$ and $b = 31.5433$ for **I** and $a = 0.0354$ and $b = 26.8182$ for **II**.

TABLE 2
Final Atomic Coordinates [$\times 10^4$] and Equivalent Isotropic Displacement Parameters [$Å^2 \times 10^3$] for I, $[C_6N_2H_{14}][Fe_2^{III}F_2(HPO_4)_2(H_2PO_4)_2]\cdot 2H_2O$

Atom	x	y	z	U_{eq}[a]
Fe(1)	2473(2)	1658(1)	7495(1)	10(1)
P(1)	461(3)	770(1)	8974(1)	14(1)
P(2)	4673(3)	2557(1)	6039(2)	19(1)
O(1)	− 1372(8)	997(3)	8424(4)	25(2)
O(2)	2112(7)	1115(3)	8621(4)	21(1)
O(3)	3563(7)	2374(3)	8335(4)	20(1)
O(4)	2942(8)	2217(3)	6329(4)	21(1)
F(1)[b]	0	2065(3)	7500	16(1)
F(2)[b]	5000	1285(3)	7500	16(1)
O(5)	464(8)	837(3)	10063(4)	24(1)
O(6)	649(8)	22(3)	8748(4)	23(1)
O(7)	4294(8)	3297(3)	6094(4)	31(2)
O(8)	4965(9)	2397(3)	4969(4)	31(2)
N(1)	4228(9)	− 871(4)	8246(5)	24(2)
C(1)	4712(29)	− 224(7)	8025(14)	142(10)
C(2)	5941(24)	− 1252(12)	8378(10)	160(12)
C(3)	3000(20)	− 1164(10)	7481(9)	112(8)

[a] U_{eq} is defined as one-third of the trace of the orthogonalized U_{ij} tensor.
[b] Site occupancy factor (SOF) = 0.5.

between 25 and 800°C. The study indicates that the weight loss occurs in two steps for **I** and in three steps for **II**. The total mass loss of 33.5% in the case of **I** corresponds well with the loss of water, amine, fluorine and condensation of the phosphate (calcd. 34.9%) and a mass loss of 30.1% in the case of **II** corresponds with the loss of the water, amine, fluorine and the condensation of the phosphate (calcd. 33%). In both the cases, the loss of the amine molecule resulted in the collapse of the framework structure, leading to the formation of largely amorphous weakly diffracting materials (XRD) that correspond to dense iron phosphate phases [$Fe_2P_2O_7$], consistent with the structures.

TABLE 3
Selected Bond Distances in I, $[C_6N_2H_{14}][Fe_2^{III}F_2(HPO_4)_2(H_2PO_4)_2]\cdot 2H_2O$

Bond	Distance, Å	[BVS][a]	Bond	Distance, Å	BVS
Fe(1)–O(1)#1	1.961(5)	[0.579]	P(1)–O(5)	1.523(6)	[1.289]
Fe(1)–O(2)	1.971(5)	[0.564]	P(1)–O(6)	1.577(6)	[1.114]
Fe(1)–O(3)	1.975(5)	[0.558]			[5.014]
Fe(1)–O(4)	2.053(5)	[0.452]	P(2)–O(3)#2	1.494(6)	[1.394]
Fe(1)–F(1)	1.974(3)	[0.451]	P(2)–O(4)	1.535(6)	[1.212]
Fe(1)–F(2)	1.981(2)	[0.442]	P(2)–O(7)	1.546(6)	[1.248]
		[3.045]	P(2)–O(8)	1.569(6)	[1.138]
P(1)–O(1)	1.513(6)	[1.325]			[4.992]
P(1)–O(2)	1.524(6)	[1.286]			
		Organic amine			
N(1)–C(1)	1.42(2)		C(1)–C(1)#2	1,57(3)	
N(1)–C(2)	1.46(2)		C(2)–C(3)#2	1.52(2)	
N(1)–C(3)	1.426(13)				

[a] BVS = bond valence sum.
#1 $-x, y, -z+\frac{3}{2}$; #2 $-x+1, y, -z+\frac{3}{2}$

SINGLE CRYSTAL STRUCTURE DETERMINATION

A suitable colorless single crystal of each compound was carefully selected under a polarizing microscope and glued to a thin glass fiber with cyanoacrylate (superglue) adhesive. Crystal structure determination by X-ray diffraction was performed on a Siemen's SMART-CCD diffractometer equipped with a normal focus, 2.4 kW sealed tube X-ray source (Mo$K\alpha$ radiation, $\lambda = 0.71073$ Å) operating at 40 kV and 40 mA. A hemisphere of intensity data were collected at room temperature in 1321 frames with ω scans (width of 0.30 and exposure time of 10 s per frame) in the 2θ range of 3–46.5°. Pertinent experimental details for the structure determinations of **I** and **II** are presented in Table 1.

An absorption correction based on symmetry-equivalent reflections was applied using SADABS program (15). Other effects, such as absorption by the glass fiber, were simultaneously corrected. The structures were solved and refined by SHELXTL-PLUS suite of programs (16). The direct methods solution readily revealed sufficient fragments of the structure (Fe, P, and O) and enabled the remainder of the non-hydrogen atoms to be located from difference Fourier maps. All the hydrogen positions were initially located in the difference map and for the final refinement, the hydrogen atoms were placed geometrically and held in the riding mode. Final residuals of $R_1 = 0.06$ and $wR_2 = 0.12$ for **I**, $R_1 = 0.034$ and $wR_2 = 0.081$ for **II**, respectively, were obtained for refinements with varying atomic positions for all the atoms and anisotropic thermal parameters for all non-hydrogen atoms and isotropic thermal parameters for all the hydrogen atoms. Full-matrix-least-squares structure refinement against $|F^2|$ was carried out using the SHELXTL-PLUS (16) package of program. The final atomic coordinates, and selected bond distances for **I** are presented in Tables 2 and 3 and the atomic coordinates, and selected bond distances and angles for **II** in Tables 4–6.

RESULTS

$[C_6N_2H_{14}][Fe_2^{III}F_2(HPO_4)_2(H_2PO_4)_2]\cdot 2H_2O$, *I*

The asymmetric unit of **I** contains 18 non-hydrogen atoms as shown in Fig. 1, of which 14 atoms belong to the "framework" and 4 atoms to the "guest" species. There is one crystallographically independent Fe and two P atoms. The fluorine atoms, F(1) and F(2), occupy special position with a site occupancy of (SOF) 0.5. The iron atom bonds

TABLE 4
Final Atomic Coordinates [$\times 10^4$] and Equivalent Isotropic Displacement Parameters [$Å^2 \times 10^3$] for II, $[C_6N_2H_{14}]_2[Fe^{III}_3(OH)F_3(PO_4)(H_2PO_4)_2]_2 \cdot H_2O$

Atom	x	y	z	U_{eq}[a]
Fe(1)	1874(1)	5777(1)	1612(1)	14(1)
Fe(2)	1893(1)	8150(1)	2600(1)	14(1)
Fe(3)	− 757(1)	9293(1)	− 22(1)	11(1)
P(1)	790(1)	8273(1)	1069(1)	12(1)
P(2)	3587(1)	7708(1)	3680(1)	16(1)
P(3)	3337(1)	4840(1)	1146(1)	18(1)
O(1)	2518(2)	5373(4)	1010(2)	24(1)
O(2)	1099(2)	6863(3)	997(2)	17(1)
O(3)	1232(2)	4184(3)	1388(2)	22(1)
O(4)	2632(2)	4871(3)	2389(2)	8(1)
F(1)	1453(2)	6325(3)	2412(1)	16(1)
F(2)	2436(2)	7516(3)	1908(1)	18(1)
O(5)	1449(2)	8667(4)	3341(2)	23(1)
O(6)	2759(2)	7383(4)	3319(2)	28(1)
O(7)	968(2)	8669(3)	1843(2)	17(1)
O(8)	3547(2)	4475(4)	454(2)	18(1)
O(9)	− 1169(2)	10694(4)	− 708(2)	19(1)
O(10)	3791(2)	7284(3)	4440(2)	18(1)
F(3)	− 101(2)	10804(3)	481(1)	16(1)
O(11)	− 90(2)	8196(3)	748(2)	15(1)
O(12)	4121(3)	6950(4)	3303(2)	35(1)
O(13)	3885(2)	6028(4)	1481(2)	28(1)
O(100)[b]	5000	5048(6)	2500	31(2)
N(1)	− 871(3)	5811(4)	836(2)	20(1)
C(1)	− 1720(3)	6004(6)	700(3)	24(1)
C(2)	− 2033(3)	4841(6)	038(3)	28(1)
C(3)	− 729(4)	4669(6)	403(3)	29(1)
C(4)	− 1215(4)	3479(6)	517(3)	29(2)
N(2)	− 1445(3)	3740(5)	1168(2)	22(1)
C(5)	− 506(3)	5517(6)	1587(3)	27(1)
C(6)	− 770(3)	4127(6)	1744(3)	28(1)

[a] U_{eq} is defined as one-third of the trace of the orthogonalized U_{ij} tensor.
[b] Site occupancy factor (SOF) = 0·5.

with 4 oxygen and 2 fluorine atoms forming an octahedra with average Fe–O/F distances of 1.986 Å. The O/F–Fe–O/F bond angles are in the range 88.0(2)–178.1° (av. 107.4°). The iron atom makes four Fe–O–P linkages to two distinct P atom neighbors with an average Fe–O–P bond angle of 138.1° and two Fe–F–Fe linkages. The iron atoms are linked together through the fluorine atoms forming infinite Fe–F–Fe one-dimensional chains. Each phosphorous atom makes two P–O–Fe bond and possesses two terminal P–O linkages. The P–O distances are in the range 1.494(6)–1.577(6) Å (av. P(1)–O = 1.534, P(2)–O = 1.536 Å) and the O–P–O bond angles are in the range 106.1(3)–113.2(3)° (av. 109.5°). The terminal P(1)–O(6), P(2)–O(7) and P(2)–O(8) bonds with distances of 1.577(6), 1.546(6) and 1.569(6) Å are formally P–OH linkages. One hydrogen position near each of the oxygen atoms O(6), O(7) and O(8) was observed in the difference Fourier maps. The other terminal bond, P(1)–O(5), with a distance of 1.523(6) Å is a P=O linkage. Similar P–O bond distances and bond angles have been observed in many of the phosphate-based open-framework materials (2–10). Bond valence sum calculations (17) also agree with the above and clearly indicate that the iron atoms are in + 3 state. The complete list of bond distances along with bond valence sum (BVS) values for **I** is presented in Table 3.

The structure of **I** is built up from isolated infinite $\{[FeF(HPO_4)(H_2PO_4)]^-\}_n$ chains running along the [100] direction with the diprotonated DABCO molecules and water molecules occupying the inter-chain spaces and interact with the chains through hydrogen bonds (Fig. 2). Each $\{[FeF(HPO_4)(H_2PO_4)]^-\}_n$ unit is built up from a central core constituted by a chain of $Fe^{III}O_4F_2$ octahedra linked by their trans fluorine atoms. The HPO_4 and H_2PO_4 tetrahedra are grafted onto this chain in such a way that two consecutive octahedra are linked by two distinct tetrahedra.

TABLE 5
Selected Bond Distances in II, $[C_6N_2H_{14}]_2[Fe^{III}_3(OH)F_3(PO_4)(H_2PO_4)_2]_2 \cdot H_2O$

Bond	Distance, Å, [BVS][a]	Bond	Distance, Å, [BVS]
Fe(1)–O(1)	1.944(4) [0.6065]	Fe(3)–O(11)	2.006(3) [0.5130]
Fe(1)–O(2)	1.932(3) [0.6265]	Fe(3)–F(3)	2.016(3) [0.3968]
Fe(1)–O(3)	1.954(4) [0.5904]	Fe(3)–F(3)#4	2.021(3) [0.3886]
Fe(1)–O(4)	1.990(3) [0.5356]		[3.0598]
Fe(1)–F(1)	2.034(3) [0.3831]	P(1)–O(9)#4	1.532(4) [1.2583]
Fe(1)–F(2)	2.023(3) [0.3947]	P(1)–O(2)	1.540(4) [1.2115]
	[3.1368]	P(1)–O(7)	1.546(4) [1.2313]
Fe(2)–O(4)#1	1.925(3) [0.6385]	P(1)–O(11)	1.553(4) [1.1888]
Fe(2)–O(5)	1.947(4) [0.6016]		[4.8899]
Fe(2)–O(6)	1.972(4) [0.5623]	P(2)–O(6)	1.515(4) [1.3174]
Fe(2)–O(7)	1.997(3) [0.5256]	P(2)–O(10)	1.527(4) [1.2685]
Fe(2)–F(1)	1.988(3) [0.4338]	P(2)–O(3)#1	1.529(4) [1.2754]
Fe(2)–F(2)	2.017(3) [0.4011]	P(2)–O(12)	1.580(4) [1.1052]
	[3.1629]		[4.9665]
Fe(3)–O(8)#2	1.934(3) [0.6231]	P(3)–O(8)	1.507(4) [1.3462]
Fe(3)–O(9)	1.962(3)[0.5777]	P(3)–O(1)	1.533(4) [1.2380]
Fe(3)–O(10)#3	1.959(3) [0.5824]	P(3)–O(5)#5	1.538(4) [1.2549]
		P(3)–O(13)	1.578(4) [1.1111]
			[4.9502]
	Organic amine		
N(1)–C(1)	1.503(7)	N(1)–C(3)	1.500(7)
N(1)–C(5)	1.498(7)	C(1)–C(2)	1.535(8)
C(3)–C(4)	1.537(8)	N(2)–C(4)	1.500(7)
N(2)–C(2)	1.507(7)	N(2)–C(6)	1.485(7)
C(5)–C(6)	1.534(8)		

[a] [BVS] = bond valence sum.
#1 $-x+\frac{1}{2}, y+\frac{1}{2}, -z+\frac{1}{2}$; #2 $x-\frac{1}{2}, y+\frac{1}{2}, z$; #3 $x-\frac{1}{2}, -y+\frac{3}{2}, z-\frac{1}{2}$; #4 $-x, -y+2, -z$; #5 $-x+\frac{1}{2}, y-\frac{1}{2}, -z+\frac{1}{2}$.

TABLE 6
Selected Bond Angles in II,
$[C_6N_2H_{14}]_2[Fe^{III}_3(OH)F_3(PO_4)(H_2PO_4)_2]_2 \cdot H_2O$

Moiety	Angle, (°)	Moiety	Angle, (°)
O(2)–Fe(1)–O(1)	100.3(2)	O(11)–Fe(3)–F(3)	82.96(13)
O(1)–Fe(1)–O(3)	96.4(2)	O(8)#2–Fe(3)–F(3)#4	176.34(14)
O(2)–Fe(1)–O(3)	91.6(2)	O(10)#3–Fe(3)–F(3)#4	88.26(13)
O(2)–Fe(1)–O(4)	168.99(14)	O(9)–Fe(3)–F(3)#4	84.70(13)
O(1)–Fe(1)–O(4)	89.18(14)	O(11)–Fe(3)–F(3)#4	86.92(13)
O(3)–Fe(1)–O(4)	92.79(14)	F(3)–Fe(3)–F(3)#4	80.72(12)
O(2)–Fe(1)–F(2)	85.54(13)	Fe(1)–O(1)–P(3)	133.2(2)
O(1)–Fe(1)–F(2)	91.10(14)	Fe(1)–O(2)–P(1)	132.6(2)
O(3)–Fe(1)–F(2)	172.32(14)	Fe(1)–O(3)–P(2)#5	132.8(2)
O(4)–Fe(1)–F(2)	88.78(13)	Fe(1)–O(4)–Fe(2)#5	128.9(2)
O(2)–Fe(1)–F(1)	89.07(13)	Fe(2)–O(5)–P(3)#1	129.2(2)
O(1)–Fe(1)–F(1)	165.69(14)	Fe(2)–O(6)–P(2)	138.8(2)
O(3)–Fe(1)–F(1)	94.02(14)	Fe(2)–O(7)–P(1)	126.5(2)
O(4)–Fe(1)–F(1)	80.57(12)	Fe(3)#6–O(8)–P(3)	142.4(2)
F(2)–Fe(1)–F(1)	78.81(11)	Fe(3)–O(9)–P(1)#4	132.9(2)
O(4)#1–Fe(2)–O(5)	91.9(2)	Fe(3)#7–O(10)–P(2)	136.3(2)
O(4)#1–Fe(2)–O(6)	94.3(2)	Fe(3)–O(11)–P(1)	128.8(2)
O(5)–Fe(2)–O(6)	87.8(2)	Fe(1)–F(1)–Fe(2)	100.33(12)
O(4)#1–Fe(2)–F(1)	168.58(13)	Fe(1)–F(2)–Fe(2)	99.73(12)
O(5)–Fe(2)–F(1)	99.22(14)	Fe(3)–F(3)–Fe(3)#4	99.29(12)
O(6)–Fe(2)–F(1)	88.76(14)	O(9)#4–P(1)–O(2)	110.6(2)
O(4)#1–Fe(2)–O(7)	93.21(14)	O(9)#4–P(1)–O(7)	107.8(2)
O(5)–Fe(2)–O(7)	94.2(2)	O(2)–P(1)–O(7)	110.4(2)
O(6)–Fe(2)–O(7)	172.1(2)	O(9)#4–P(1)–O(11)	112.6(2)
F(1)–Fe(2)–O(7)	83.40(13)	O(2)–P(1)–O(11)	106.0(2)
O(4)#1–Fe(2)–F(2)	89.16(13)	O(7)–P(1)–O(11)	109.5(2)
O(5)–Fe(2)–F(2)	174.11(14)	O(6)–P(2)–O(10)	110.6(2)
O(6)–Fe(2)–F(2)	86.4(2)	O(6)–P(2)–O(3)#1	112.1(2)
F(1)–Fe(2)–F(2)	80.05(11)	O(10)–P(2)–O(3)#1	111.1(2)
O(7)–Fe(2)–F(2)	91.57(13)	O(6)–P(2)–O(12)	109.3(2)
O(8)#2–Fe(3)–O(10)#3	95.4(2)	O(10)–P(2)–O(12)	109.5(2)
O(8)#2–Fe(3)–O(9)	95.1(2)	O(3)#1–P(2)–O(12)	104.2(2)
O(9)–Fe(3)–O(10)#3	99.8(2)	O(8)–P(3)–O(1)	107.6(2)
O(8)#2–Fe(3)–O(11)	92.44(14)	O(8)–P(3)–O(5)#5	110.9(2)
O(10)#3–Fe(3)–O(11)	93.15(14)	O(1)–P(3)–O(5)#5	115.9(2)
O(9)–Fe(3)–O(11)	164.34(14)	O(8)–P(3)–O(13)	109.8(2)
O(8)#2–Fe(3)–F(3)	95.63(13)	O(1)–P(3)–O(13)	106.3(2)
O(10)#3–Fe(3)–F(3)	168.48(14)	O(5)#5–P(3)–O(13)	106.1(2)
O(9)–Fe(3)–F(3)	82.65(13)		
	Organic amine		
C(5)–N(1)–C(3)	109.5(4)	C(5)–N(1)–C(1)	110.8(4)
C(3)–N(1)–C(1)	109.0(4)	N(1)–C(5)–C(6)	107.9(4)
N(2)–C(6)–C(5)	108.4(4)	C(6)–N(2)–C(4)	110.7(5)
C(6)–N(2)–C(2)	109.7(4)	C(4)–N(2)–C(2)	109.4(4)
N(2)–C(4)–C(3)	107.7(4)	N(1)–C(3)–C(4)	107.8(4)
N(2)–C(2)–C(1)	107.4(5)	N(1)–C(1)–C(2)	108.1(4)

#1 $-x+\frac{1}{2}, y+\frac{1}{2}, -z+\frac{1}{2}$; #2 $x-\frac{1}{2}, y+\frac{1}{2}, z$; #3 $x-\frac{1}{2}, -y+\frac{3}{2}, z-\frac{1}{2}$; #4 $-x, -y+2, -z$; #5 $-x+\frac{1}{2}, y-\frac{1}{2}, -z+\frac{1}{2}$; #6 $x+\frac{1}{2}, y-\frac{1}{2}, z$; #7 $x+\frac{1}{2}, -y+\frac{3}{2}, z+\frac{1}{2}$.

Similar connectivity involving the octahedral and tetrahedral units has been encountered in many mineralogical structures related to tancoite (12). The projection of the structure down the chain axis, showing the layout of adjacent chains is given in Fig. 3. It may be noted that strong intra- and inter-chain hydrogen bond interactions exist between the adjacent chains, through the terminal hydroxyl groups. Such hydrogen bond interactions lend additional structural stability in **I**. The complete list of the hydrogen bond interactions is listed in Table 7.

$[C_6N_2H_{14}]_2[Fe^{III}_3(OH)F_3(PO_4)(HPO_4)_2]_2 \cdot H_2O$, **II**

The asymmetric unit contains 31 non-hydrogen atoms as shown in Fig. 4, of which 22 atoms belong to the "framework" and 9 atoms to the "guest" molecules. There are three crystallographically independent Fe and P atoms. The iron atoms are octahedrally coordinated by 4 oxygen atoms and 2 fluorine atoms with Fe–O/F distances in the range 1.925(3)–2.034(3) Å (av. Fe(1)–O/F = 1.979, Fe(2)–O/F = 1.974, Fe(3)–O/F = 1.983 Å). The O/F–Fe–O/F bond angles are in the range 78.81(11)–176.34(14)° (av. O/F–Fe(1) –O/F = 105.7, O/F–Fe(2)–O/F = 106.3, O/F–Fe(3)–O/F = 105.8°) Of the three Fe atoms, Fe(1) and Fe(2) make three Fe–O–P bonds and Fe(3) makes four such bonds with an average Fe–O–P bond angle of 133.4°. The other three connections needed for the octahedral linkage in the cases of Fe(1) and Fe(2) come from F and –OH bridges and through F bridges for Fe(3). An average Fe–F–Fe bond angle of 99.78° and Fe–OH–Fe of 128.9° result from such bonds. Of the three P atoms, P(1) makes four P–O–Fe linkages and P(2) and P(3) make only three P–O–Fe connections and possess one terminal bond. The P–O distances are in the range 1.507(4)–1.580(4) Å (av. P(1)–O = 1.543, P(2)–O = 1.538, P(3)–O = 1.539 Å) and O–P–O bond angles are in the range 104.2(2)–115.9(2)° (av. 109.5°). The terminal P(2)–O(12) and P(3)–O(13) bonds with distances of 1.580(4) and 1.578(4) Å are P–OH linkages. One hydrogen position near each of the oxygen atoms O(12) and O(13) was observed in the difference Fourier maps. Similar P–O bond distances and bond angles have been routinely encountered in open-framework phosphates (2–10). Bond valence sum calculations (17) also agree with the above and clearly indicate that the iron atoms are in + 3 state. The complete list of bond distances and angles along with bond valence sum (BVS) values for **II** is presented in Tables 5 and 6.

As mentioned earlier, the framework structure of **II** is similar to that of the gallium phosphate, $[C_6N_2H_{14}]_2[Ga_3(OH)F_3(PO_4)(HPO_4)_2]_2 \cdot H_2O$ (13), and is built up from the linkages between the $Fe(1,2)O_3(OH)F_2$, $Fe(3)O_4F_2$ and PO_4 polyhedral units. The connectivity between Fe(1) and Fe(2) through F(1) and F(2) is such that it forms an edge-shared Fe(1)–μ[F(1),F(2)]–Fe(2) bond to form an $Fe_2F_2O_8$ dimer. These dimeric units are connected together through their corners via μ[O(4)H] oxygen atom to form an infinite Fe–O/F–Fe sinusoidal polymeric chains as shown in Figure 5a. The one-dimensional chains are further linked to each other via phosphate groups, [P(1)O_4 and P(2)O_4], attached with another dimeric unit formed by $Fe(3)O_4F_2$,

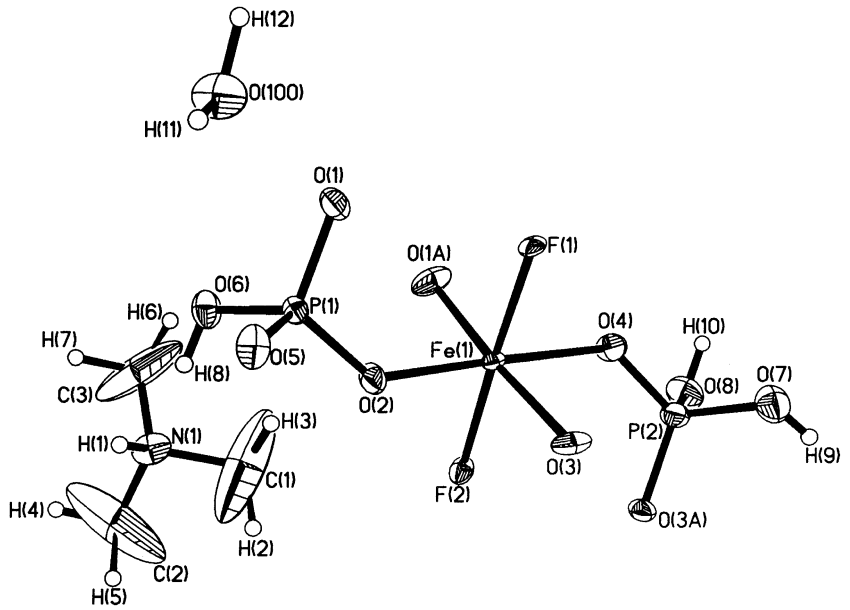

FIG. 1. ORTEP plot of **I**, $[C_6N_2H_{14}][Fe_2^{III}F_2(HPO_4)_2(H_2PO_4)_2]\cdot 2H_2O$, showing the asymmetric unit. Thermal ellipsoids are given at 50% probability.

described as SBU-4 (Fig. 5b) by Ferey (18). This connectivity between the chain and the SBU-4 unit results in a layer with 3-, 6- and 8-membered apertures as shown in Fig. 6. The $P(3)O_4$ units cross-link these layers forming a three-dimensional structure with 8-membered channels along the [010] direction (Fig. 7). The water molecules occupy the center of this channel. The connectivity between the various polyhedral units also results in 8-membered channels along [100] and [001] directions as well. Thus, **II**, is truly three-dimensional with channels along all the crystallographic axes. **II**

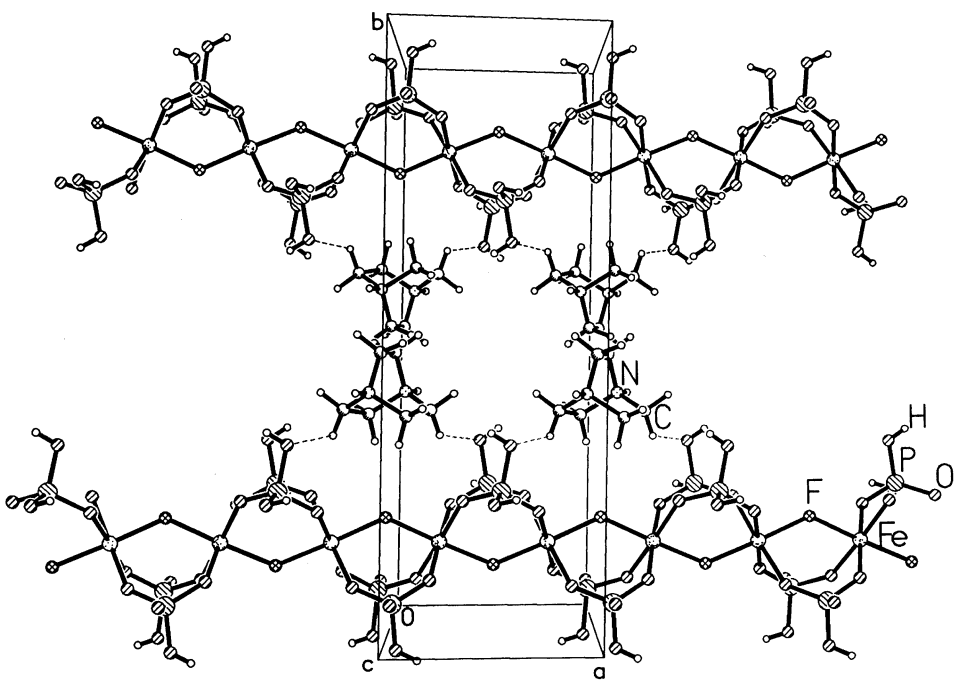

FIG. 2. Structure of **I** in the *ab* plane showing the tancoite chains and the amine molecules. The dotted lines represent the hydrogen bond interactions.

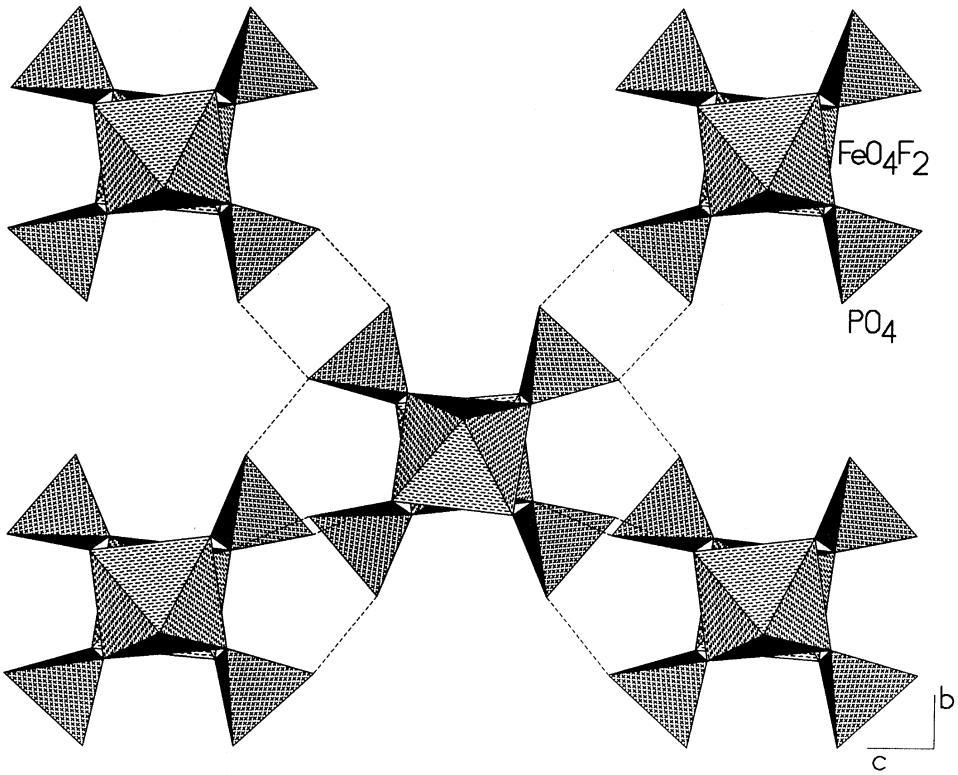

FIG. 3. View of the structure of **I** along the chain axis. The dotted lines represent the hydrogen bond interactions.

TABLE 7
Important Hydrogen Bond Interactions in I, $[C_6N_2H_{14}][Fe_2^{III}F_2(HPO_4)_2(H_2PO_4)_2]\cdot 2H_2O$, II, and $[C_6N_2H_{14}]_2[Fe_3^{III}(OH)F_3(PO_4)(HPO_4)_2]_2\cdot H_2O$

Moiety	Distance Å	Moiety	Angle (°)
		I	
O(100)–H(1)	1.958(9)	O(100)–H(1)–N(1)	145.5(7)
O(5)–H(9)[a]	1.834(8)	O(5)–H(9)–O(7)[a]	137.6(7)
O(4)–H(10)[a]	1.888(8)	O(4)–H(10)–O(8)[a]	172.2(8)
N(1)–H(11)	1.78(5)	N(1)–H(11)–O(100)	162(14)
O(2)–H(12)	2.03(8)	O(2)–H(12)–O(100)	171(9)
O(5)–H(5)	2.359(16)	O(5)–H(5)–C(2)	155.9(15)
		II	
O(11)–H(14)	1.921(6)	O(11)–H(14)–N(1)	163.2(5)
O(6)–H(20)[a]	2.16(11)	O(6)–H(20)–O(4)[a]	158(10)
O(7)–H(30)[a]	2.493(5)	O(7)–H(30)–O(12)[a]	165.7(6)
O(7)–H(101)	1.96(8)	O(7)–H(101)–O(100)	176(8)
O(5)–H(1)	2.352(7)	O(5)–H(1)–C(1)	151.8(6)
O(9)–H(3)	2.386(7)	O(9)–H(3)–C(2)	139.9(6)
F(1)–H(4)	2.531(7)	F(1)–H(4)–C(2)	140.6(6)
F(3)–H(7)	2.411(7)	F(3)–H(7)–C(4)	168.2(7)
F(1)–H(11)	2.296(7)	F(1)–H(11)–C(5)	138.1(6)

[a] Intra-framework.

also possesses extensive intra-framework hydrogen bond interactions between the terminal hydroxyl groups, and between the framework oxygen atoms, water, and amine molecules. The complete list of hydrogen bond interactions in **II** is presented in Table 7.

DISCUSSION

Two new iron(III) phosphates, **I**, $[C_6N_2H_{14}][Fe_2^{III}F_2(HPO_4)_2(H_2PO_4)_2]\cdot 2H_2O$, **II**, and $[C_6N_2H_{14}]_2[Fe_3^{III}(OH)F_3(PO_4)(HPO_4)_2]_2\cdot H_2O$ have been obtained as good quality single crystals by hydrothermal methods. Whilst **I** is one-dimensional, **II** is three-dimensional in nature. Although the structures of both **I** and **II** are formed from the expected polyhedral building units, distinct differences exist between them. The syntheses of both the compounds were carried out by minor variations in the synthesis mixture, especially the temperature. As is typical of kinetic-controlled solvent-mediated reactions, there is no correlation between the starting composition and the majority solid-phase product. The isolation of the one-dimensional structure at a lower temperature (100°C) probably indicates that it could be the precursor for the higher temperature (150°C) three-dimensional phase. This observation becomes more pertinent as it has been recently shown in

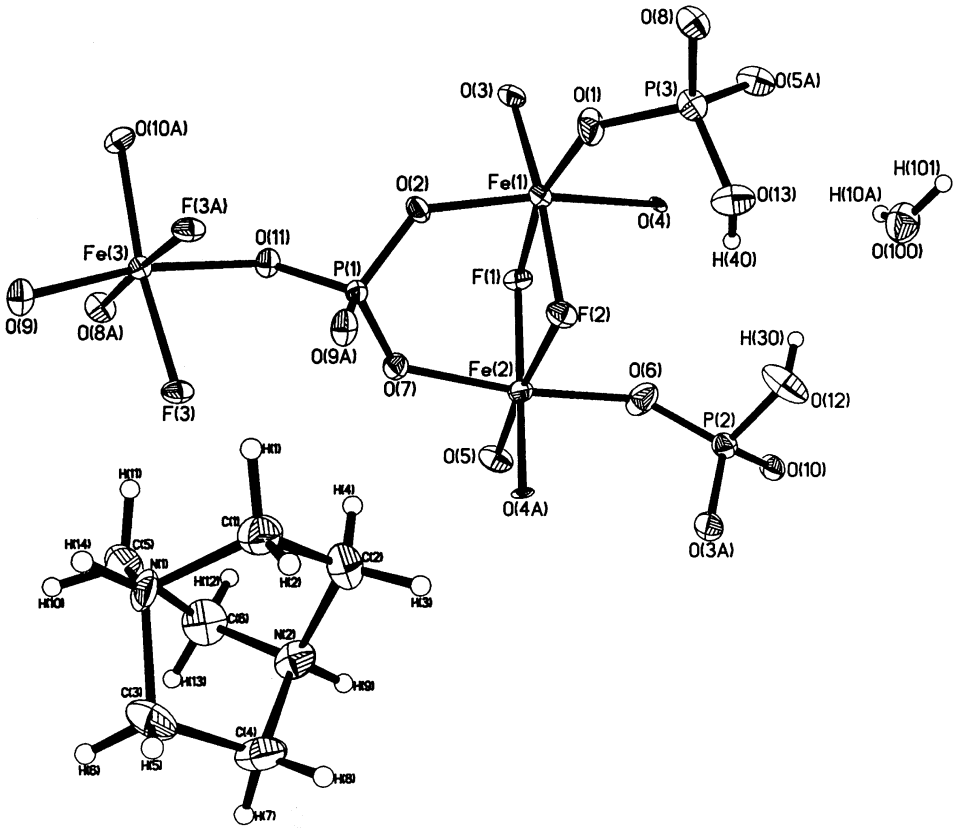

FIG. 4. ORTEP plot of **II**, $[C_6N_2H_{14}]_2[Fe^{III}_3(OH)F_3(PO_4)(HPO_4)_2]_2{\cdot}H_2O$. Symmetry-generated atoms are also labeled. Thermal ellipsoids are given at 50% probability.

zinc phosphates, that the lower dimensional solids are more reactive and readily transform into higher dimensional ones under appropriate conditions (19). Based on these transformation reactions of the zinc phosphates, Rao *et al.* (19b) have also proposed an *aufbau* principle for the building up of open structures, wherein the lower dimensional solid undergoes transformation into higher dimensional ones.

Compounds **I** and **II** are formed from FeO_4F_2 octahedra and PO_4 tetrahedra linked to form one- and three-dimensional structures. The common structural feature in both **I** and **II** is the presence of infinite one-dimensional chains of Fe–O/F–Fe formed by the FeO_4F_2 octahedra. Whilst the linear chains in **I** are formed by the corner sharing of FeO_4F_2 octahedra through the Fe–μ(F)–Fe linkages, the sinusoidal chains in **II** are formed by two edge-shared octahedral dimers, formed by the linkage of two iron atoms by two fluorine atoms, connected through their corners by Fe–μ(OH)–Fe linkage. This type of connectivity between the Fe octahedra, in **II**, is unusual and has not been encountered previously in any of the iron phosphates reported so far (2–10). In addition to the commonality between the structures of **I** and **II**, the structures themselves merit comparison with other known phases possessing similar structural features.

As mentioned earlier, the structure of **I** is similar to that of tancoite. Tancoite is a phosphate mineral of the formula, $LiNa_2HAl(PO_4)_2(OH)$, possessing one-dimensional chain structure, discovered at the Tanco Mine, Bernic Lake, Manitoba (20). These type of chains have been encountered in many phosphate, sulfate and silicate minerals (16). The chains generally have the composition, $[M(TO_4)_2L]_n$ (M and T are cations of different coordination, usually octahedral and tetrahedral, L = anionic ligand, e.g., O^{2-}, OH^- or F^-). Iron phosphates with tancoite chains have also been reported in the literature with compositions of $[N_2C_3H_{12}][FeF(HPO_4)_2]{\cdot}xH_2O$ ($x = 0.2$) (3a) and $[C_2N_2H_{10}][Fe(OH)(HPO_4)_2]$ (3c) prepared in the presence of different amines. It is to be noted that both the phosphate groups in these iron phosphates are similar possessing one terminal P–OH linkages, and the difference between the two structures are the way the iron atoms are linked. Whilst in the former, it is through a fluoride bridge, in the latter it is through a hydroxyl group. In **I**, we have similar connectivity with the iron atoms being bridged by their corner via a fluoride ion, but the composition of **I**, $[C_6N_2H_{14}][Fe^{III}_2F_2$

$(HPO_4)_2(H_2PO_4)_2]\cdot 2H_2O$, is different compared to the above two iron phosphates. The phosphates groups in **I** are differently protonated. This type of differential protonation of the phosphate groups in **I**, also has not been encountered in any of the reported structures of Al and Ga phosphates possessing tancoite chains (21). It is likely that the modified synthetic approach of using a coordination complex as the starting source of iron may have played a role in forming the tancoite chain with a new composition. Additionally, **I** could also be reactive as it possesses terminal –OH groups associated with the $PO_3(OH)$ and $PO_2(OH)_2$ moieties and can be condensed to form two- and three-dimensiona

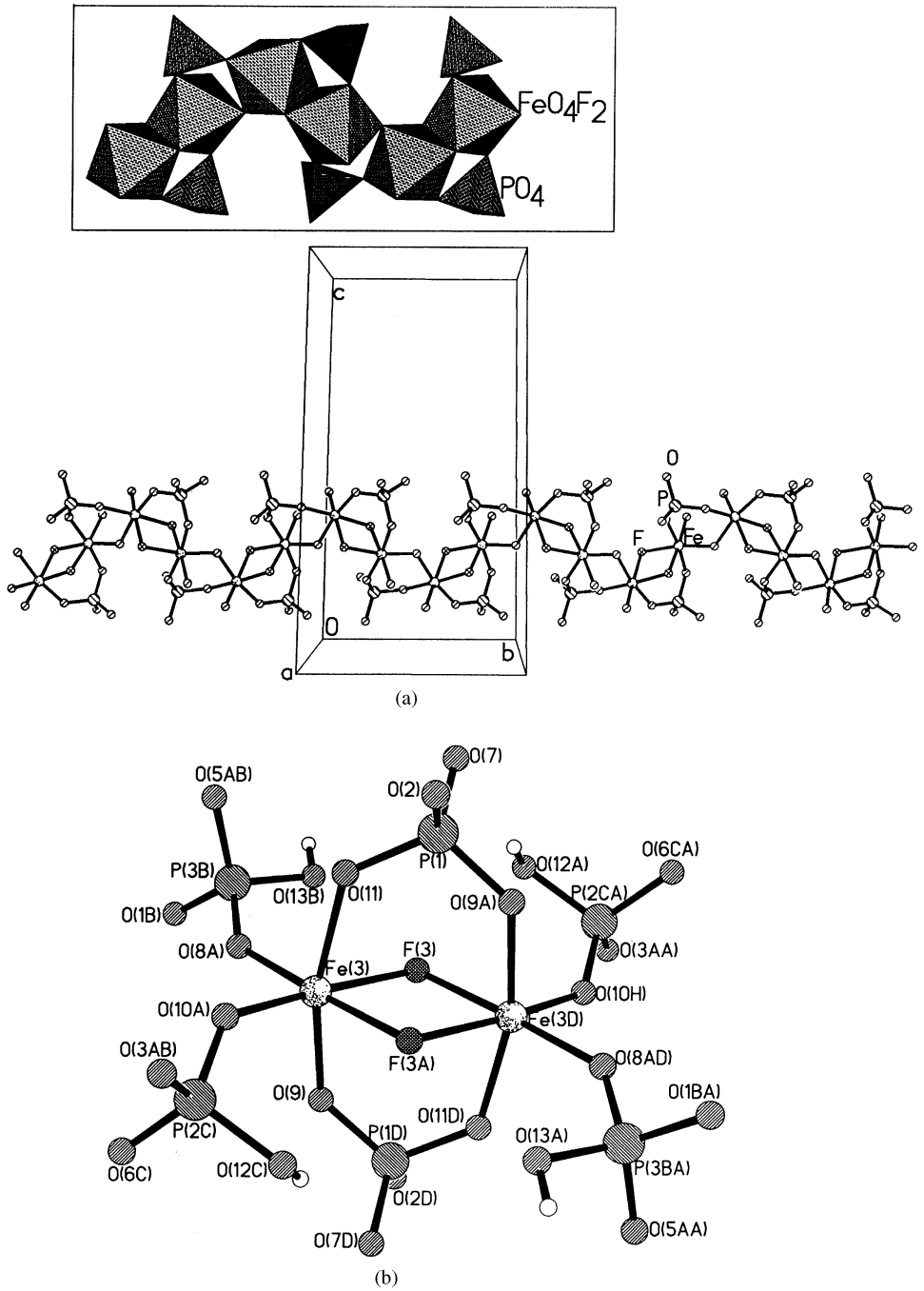

FIG. 5. (a) Structure of **II** showing one of the building units. The inset shows the polyhedral view of a section of the chain. Note the edge and corner shared $Fe(F/O)_6$ octahedra. (b) The secondary building unit, SBU-4, observed in **II**. The SBU-4 connects the chains to form the layer.

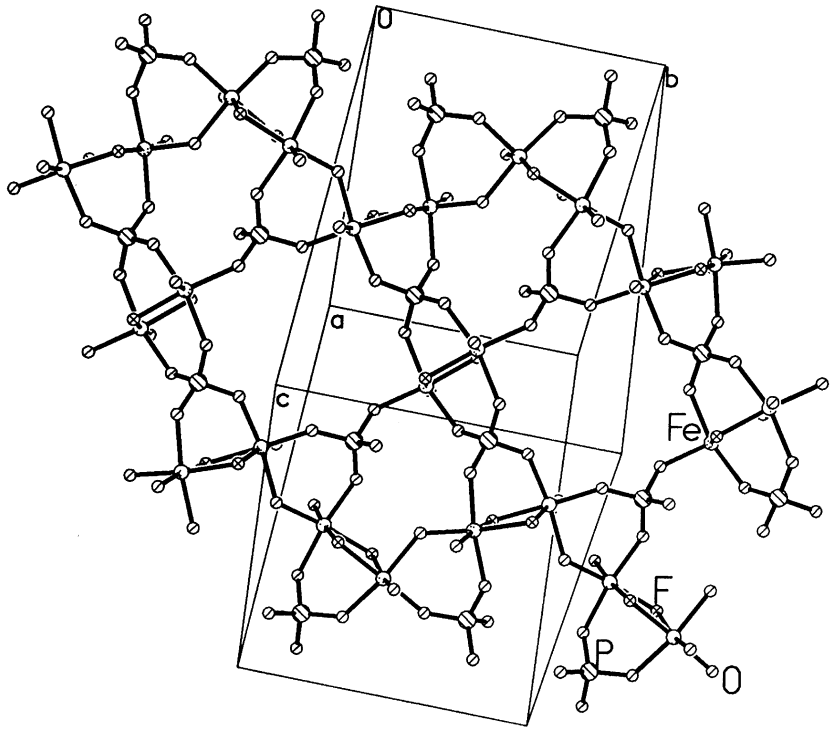

FIG. 6. Structure of **II** showing a single layer. These layers are cross-linked by PO_4 tetrahedra forming the three-dimensional structure.

architectures by the elimination of water molecules under appropriate conditions. Such reactive transformations have been employed for the understanding of formation and preparation of new phosphates of zinc in recent years (19).

The structure of **II** is formed by interconnecting $Fe_2O_7(OH)F_2$ bi-octahedra, sharing edges and connected through their corners, with FeO_4F_2 octahedra via the PO_4 tetrahedra. Although this is the first time such connectivity between the polyhedral units has been observed in

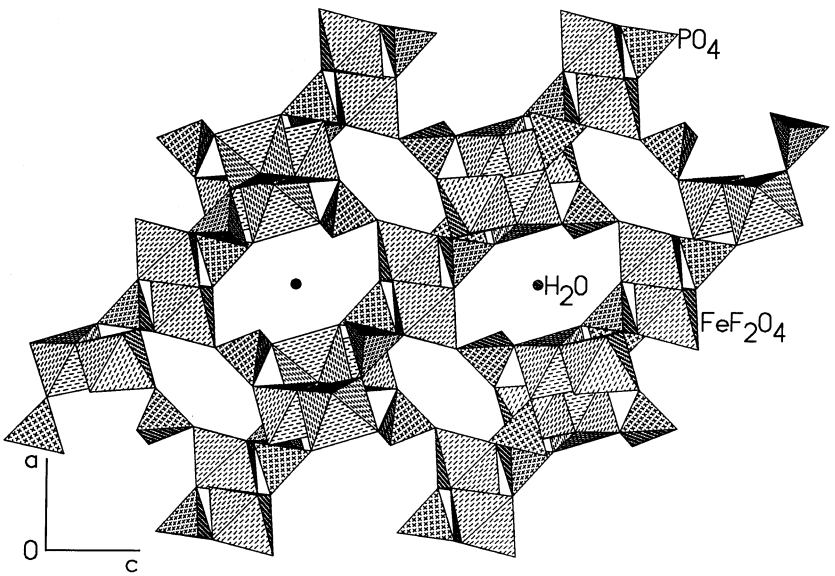

FIG. 7. Structure of **II** along the *b* axis. Note the formation of 8-membered channels. Water molecules occupy the center of the channels. Amine molecules are not shown.

open-framework iron phosphates, similar framework connectivity has been encountered earlier in a gallophosphate, ULM-1 (12). Recently, the structure of **II** has been described in an iron arsenate synthesized in the presence of DABCO (22). The iron phosphate analogue, however, has not been prepared. The polymeric one-dimensional Fe–O/F–Fe chain, observed in **II**, has close similarity with that described earlier in another iron phosphate, $[C_4N_3H_{16}][C_4N_3H_{15}][Fe^{III}_5F_4(H_2PO_4)(HPO_4)_3(PO_4)_3]\cdot H_2O$, where edge and corner sharing of FeO_4F_2 octahedral units has been observed. Additionally, this iron phosphate also possesses iron phosphate layers separated and cross-linked by PO_4 tetrahedral units, as in **II**; the main difference between the two structures being the formation of an extra large 24-member tunnels in $[C_4N_3H_{16}][C_4N_3H_{15}][Fe^{III}_5F_4(H_2PO_4)(HPO_4)_3(PO_4)_3]\cdot H_2O$, compared to 8-membered channels in **II**. Eight-membered channels are quite common in many of the phosphate-based open-framework materials (1).

CONCLUSIONS

In summary, the syntheses and structures of two new iron phosphates, **I**, $[C_6N_2H_{14}][Fe^{III}_2F_2(HPO_4)_2(H_2PO_4)_2]\cdot 2H_2O$, **II**, and $[C_6N_2H_{14}]_2[Fe^{III}_3(OH)F_3(PO_4)(HPO_4)_2]_2\cdot H_2O$ have been accomplished using hydrothermal methods employing organic complexes as the source for iron. These and the earlier reported iron phosphate structures (7b, 7c) clearly indicate the merits of using unusual complex precursors as the starting source for the metal ions. Our preliminary transformation reactions of **I** indicate that it is reactive and transforms into new types of iron phosphate phases. We are currently pursuing this lead further to understand the mechanism of formation of these solids.

ACKNOWLEDGMENTS

The authors thank Prof. C.N.R. Rao, FRS for his kind help, support and encouragement. SM thanks JNCASR for the award of a summer research fellowship. SN thanks the Council of Scientific and Industrial Research (CSIR), Govt. of India for the award of a research grant. SN also thanks The Royal Society of Chemistry for the award of *JWT Jones Traveling Fellowship*.

REFERENCES

1. A. K. Cheetham, G. Ferey, and T. Loiseau, *Angew. Chem. Int. Ed.* **38,** 3268 (1999).
2. K.-H. Lii, Y.-F. Huang, V. Zima, C.-Y. Huang, H.-M. Lin, J.-C. Jiang, F.-L. Liao, and S. L. Wang, *Chem. Mater.* **10,** 2599 (1998) and references therein.
3. (a) M. Cavellec, D. Riou, J.-M. Greneche and G. Ferey, *Inorg. Chem.* **36,** 2187 (1997); (b) V. Zima and K.-H. Lii, *J. Chem. Soc., Dalton Trans.* 4109 (1998); (c) Z. A. D. Lethbridge, P. Lightfoot, R. E. Morris, D. S. Wragg, P. A. Wright, Å. Kvick, and G. Vaughan, *J. Solid State Chem.* **142,** 455 (1999).
4. (a) M. Cavellec, D. Riou and G. Ferey, *J. Solid State Chem.* **112,** 441 (1994); (b) M. Cavellec, D. Riou, and G. Ferey, *Eur. J. Solid State Inorg. Chem.* **32,** 271 (1995); (c) M. Cavellec, D. Riou, and G. Ferey, *Acta Crystallogr. C* **51,** 2242 (1995); (d) M. R. Cavellec, J. M. Greneche, D. Riou, and G. Ferey *Chem. Mater.* **10,** 1914 (1998).
5. (a) J. R. D. DeBord, W. M. Reiff, R. C. Haushalter, and J. Zubieta, *J. Solid State Chem.* **125,** 186 (1996); (b) K.-H. Lii and Y.-F. Huang, *Chem. Commun.* 1311 (1997); (c) V. Zima, K.-H. Lii, N. Nguyen, and A. Ducouret, *Chem. Mater.* **10,** 1914 (1998).
6. (a) A. Mgaidi, H. Boughzala, A. Driss, R. Clerac, and C. Coulon, *J. Solid State Chem.* **144,** 163 (1999); (b) A.R. Cowley and A.M. Chippindale, *J. Chem. Soc. Dalton Trans.*, 3425 (2000).
7. (a) A. Choudhury, S. Natarajan, and C. N. R. Rao, *Chem. Commun.* 1305 (1999); (b) A. Choudhury and S. Natarajan, *Int. J. Inorg. Chem.* **2,** 217 (2000); (c) A. Choudhry and S. Natarajan, *J. Solid State Chem.* **154,** 507 (2000).
8. (a) M. Cavellec, D. Riou, and G. Ferey, *Inorg. Chim. Acta.* **291,** 317 (1999); (b) M. Cavellec, D. Riou, J.-M. Greneche, and G. Ferey, *J. Magn. Magn. Mater.* **163,** 173 (1996); (c) M. Cavellec, D. Riou, C. Ninclaus, J.-M. Greneche, and G. Ferey, *Zeolites.* **17,** 250 (1996); (d) M. Cavellec, C. Egger, J. Linares, M. Nogues, F. Varret, and G. Ferey, *J. Solid State Chem.* **134,** 349 (1997); (e) M. Cavellec, J.-M. Greneche, D. Riou, and G. Ferey, *Microporous Mater.* **8,** 103 (1997); (f) M. Cavellec, J.-M. Greneche, and G. Ferey, *Microporous Mesoporous Mater.* **20**, 45 (1998).
9. (a) K.-H. Lii and Y.-F. Huang, *Chem. Commun.* 839 (1997); (b) K.-H. Lii and Y-F. Huang, *J. Chem. Soc., Dalton Trans.* 2221 (1997); (c) C.-Y. Huanh, S.-L. Wang, and K.-H. Lii, *J. Porous Mater.* **5,** 147 (1998); (d) V. Zima and K.-H. Lii, *J. Solid State Chem.* **139,** 326 (1998).
10. J. R. D. DeBord, W. M. Reiff, C. J. Warren, R. C. Haushalter, and J. Zubieta, *Chem. Mater.*, **9,** 1994 (1997).
11. S. Neeraj and S. Natarajan, *Int. J. Inorg. Mater.* **1,** 317 (1999).
12. F. C. Hawthorne, *Acta Crystallogr. Sect. B* **50,** 481 (1994) and references therein.
13. T. Liseau and G. Ferey, *J. Chem. Soc., Chem. Commun.* 1197 (1992).
14. G. H. Jeffery, J. Bassett, J. Mendham, and R. C. Denney, Vogel's Textbook of Quantitative Chemical Analysis. Vth ed. John Wiley and Sons Inc., New York, 1989.
15. G. M. Sheldrick, SADABS Siemens Area Detector Absorption Correction Program. University of Gottingen, Gottingen, Germany.
16. G. M. Sheldrick, "SHELXTL-PLUS Program for Crystal Structure Solution and Refinement." University of Gottingen, Gottingen, Germany, 1993.
17. I. D. Brown and D. Altermatt, *Acta Crystallogr., Sec. B* **41,** 244 (1984).
18. (a) G. Ferey, *J. Fluroine Chem.* **72,** 187 (1995); (b) G. Ferey, *C.R. Acad. Sci. Ser.* II, 1 (1998); (c) G. Ferey, *J. Solid State Chem.* **152,** 37 (2000); (d) G. Ferey, *Chem. Mater.* **13,** 3084 (2001).
19. (a) C. N. R. Rao, S. Natarajan, and S. Neeraj, *J. Solid State Chem.* **152,** 302 (2000); (b) C. N. R. Rao, S. Natarajan, A. Choudhury, S. Neeraj, and A. A. Ayi, *Acc. Chem. Res.* **34,** 80 (2001); (c) C. N. R. Rao, S. Natarajan, A. Choudhury, S. Neeraj and R. Vaidhyanathan, *Acta. Crystallogr. Sec. B.*, **57,** 1 (2001); (d) A. A. Ayi, A. Choudhury, S. Natarajan, S. Neeraj, and C. N. R. Rao, *J. Mater. Chem.* **11,** 1181 (2001); (e) A. Choudhury, S. Neeraj, S. Natarajan, and C. N. R. Rao, *J. Mater. Chem.* **11,** 1537 (2001); (f) S. Natarajan, *J. Ind. Inst. Sci.* **81,** 25 (2001); (g) A. Choudhury, S. Neeraj, S. Natarajan and C. N. R. Rao, *J. Mater. Chem.* (2002) (in press); (h) R. I. Walton, A. J. Norquist, S. Neeraj, S. Natarajan, C. N. R. Rao, and D. O'Hare, *Chem. Commun.* 1990, (2001).
20. R. A. Ramik, B. D. Sturman, P. J. Dunn, and A. S. Poverennykh, *Can. Mineral.* **18,** 185 (1980).
21. (a) T. Loiseau, F. Serpaggi, and G. Ferey, *Chem. Commun.*, 1093 (1997); (b) M. P. Attfield, R. E. Morris, I. Burshtein, C. F. Campana, and A. K. Cheetham, *J. Solid State Chem.* **118,** 412 (1995); (c)H.-M. Lin and K.-H. Lii, *Inorg. Chem.* **37,** 4220 (1998); (d)K.-H. Lii and S.-L. Wang, *J. Solid State Chem.* **128,** 21 (1997).
22. B. Bazon, J. L. Mesa, J. L. Pizarro, A. Goni, L. Lezanna, M. I. Arirortua, and T. Rojo, *Inorg. Chem.* **40,** 5691 (2001).